Interferometry with few photons

Q. Pears Stefano, ^{1,2,*} A. G. Magnoni, ^{3,1,†} D. Rodrigues, ^{1,4} J. Tiffenberg, ⁵ and C. Iemmi^{1,2}

¹ Universidad de Buenos Aires, Facultad de Ciencias Exactas y Naturales,
Departamento de Física, Pabellón I, Ciudad Universitaria (1428), Buenos Aires, Argentina

² CONICET - Universidad de Buenos Aires, Buenos Aires, Argentina.

³ Laboratorio de Óptica Cuántica, DEILAP, UNIDEF (CITEDEF-CONICET), Buenos Aires, Argentina

⁴ CONICET - Universidad de Buenos Aires, Instituto de Física de Buenos Aires (IFIBA), Buenos Aires, Argentina.

⁵ Fermi National Accelerator Laboratory, Batavia IL, United States

(Dated: February 21, 2024)

Optical phase determination is an important and established tool in diverse fields such as astronomy, biology, or quantum optics. There is increasing interest in using a lower number of total photons. However, different noise sources, such as electronic readout noise in the detector, and shot noise, hamper the phase estimation in regimes of very low illumination. Here we report a study on how the quality of phase determination is affected by these two sources of noise. To that end, we experimentally reconstruct different wavefronts by means of a point diffraction interferometer for different mean intensities of illumination, up to 15 phot/px. Our interferometer features a Skipper-CCD sensor, which allows us to reduce the readout noise arbitrarily, thus enabling us to separate the effect of these two sources of noise. For two cases of interest: a spatial qudit encoding phase, consisting of d=6 uniform phase regions, and a more general continuous phase, we see that reducing the readout noise leads to a clear improvement in the quality of reconstruction. This can be explained by a simple noise model that allows us to predict the expected fidelity of reconstruction and shows excellent agreement with the measurements.

I. INTRODUCTION

Interferometric measurements of light involve different techniques that allow to know phase distributions with high precision. Although interferometry was initially related to metrology of optical systems, its applications spread in fields as diverse as astronomy, biology, quantum optics and many more. Current advances achieved in computers and optoelectronic devices, such as spatial light modulators and detectors, make interferometry a widely used tool in a large number of applications [1–6].

Digital recording and numerical processing of an interferogram led to a great improvement in measurement techniques. It wasn't until the mid-1990s that light sensors began to provide images of a certain quality. But, once the initial objective was achieved, which was to increase their spatial resolution, the challenge of achieving images with low light levels and good signal-to-noise ratio (SNR) arose.

Two sources of noise corrupt the process of capturing an image: those that come from the source (shot noise) and those that originate from the sensor (readout noise). Even though increasing the signal (either the intensity or the exposure time) seems an obvious way to improve the SNR, there are experiences where this is not possible. Some alternative proposals include the use of unconventional light sources such as squeezed states or entangled photons [7, 8]. Unfortunately, these devices

are not easy to implement in most optical set-ups. Measurements at very low light levels have applications in diverse fields including quantum information processing or biological studies, where the sample can be damaged by a high photon flux. Some of these experiences can be performed by using, for example, a highly attenuated laser beam. In that scenario, a doubt arises: how many photons are needed to calculate a phase distribution? In order to answer that question, it would be necessary to be able to separate the noise caused by the light source statistics, from the readout noise. A direct way of doing this is by eliminating the latter using Skipper-CCD sensor [9] which, by contrast with other technologies, holds this feature in an unprecedented wide dynamic range, from zero to a thousand photons per pixel [10]. In this work, we propose to measure phase distributions at very low light levels in two different situations: in one of them we perform quantum state tomography (QST) on spatial q-dits (D-level quantum systems). In the other, we evaluate a an arbitrary phase distribution: in this case we evaluate a continuous quadratic wavefront. The phase reconstruction process is analyzed for different numbers of photons per pixel and readout noise on the Skipper-CCD.

The article is organized as follows: in section II we review the interferometric process used to obtain the phase distribution, while in section III we describe the experimental setup. In section IV, on the one hand, we numerically simulate the expected results for different light intensities, taking into account the light source statistics and the readout noise. On the other hand, the data acquisition method is explained and experimental results are analyzed. Finally, in section V we give the conclusions.

^{*} quimeymartin.pearsstefano@ehu.eus; Present address: Centro de Física de Materiales, Paseo Manuel de Lardizabal 5, 20018 Donostia-San Sebastián, Spain

[†] magnoni.agustina@gmail.com

II. METHODOLOGY FRAMEWORK

Phase-shifting interferometry (PSI) has proven to be an accurate and precise method to evaluate wavefront phase distributions. In this technique, controlled phase shifts are introduced between the reference and the tested beam [11]. The number of interferograms recorded as the phase is shifted varies depending on the algorithm employed to recover the phase distribution of the wavefront.

As it was previously mentioned, to diminish the readout noise, we used a Skipper-CCD. Although this device requires a recording time similar to that of conventional CCDs, the total acquisition time for each interferogram, including the noise reduction process $(60 \,\mu\text{sec/pixel/sample})$, makes necessary the use of a very stable interferometer. To this end, we implemented an architecture based on a point diffraction interferometer (PDI) that was introduced by Linnik [12]. Its commonpath configuration, where the reference beam is generated from the same wavefront under characterization, results on an interferometer extremely stable against vibrations and air turbulence. When combined with PSI schemes, for example by using liquid crystal technology [13–15] to control the phase steps, the potential applications of this interferometer are enhanced.

The reconstruction of the full wavefront U(x,y) is done by using a the PSI architecture similar to that described in reference [14]. Briefly, a convergent optical processor allows to apply at the Fourier Transform plane of the input wavefront U(x,y), a point-like phase filter. This element generates a diffracted beam that is used as the interferometric reference. The resulting interferograms of applying N=4 controlled phase shifts, $\alpha_n=2\pi n/N$, with $n=0,\cdots,3$, are registered with the Skipper CCD.

The resulting amplitude for each of the phase shifts α_n at the image plane Π_i is

$$E_n(x,y) = U(x,y) + |K|e^{i\mu} \left[e^{i\alpha_n} - 1 \right], \qquad (1)$$

where |K| and μ are, respectively, the amplitude and phase of the reference beam. It is worth noting that the reference beam corresponds to a plane wave with the mean value of U(x,y). To highlight that the final aim of this method is to obtain the the phase of U(x,y), it is useful to rewrite $U(x,y)=u(x,y)\exp(i\phi(x,y))$, where u(x,y) is the absolute value of U(x,y) and $\phi(x,y)$ represents the phase. With the aid of the following combination of all the interferograms

$$C(x,y) = \sum_{n=0}^{N} |E_n(x,y)|^2 \cos\left(\frac{2\pi n}{N}\right)$$
 (2)

$$S(x,y) = \sum_{n=0}^{N} |E_n(x,y)|^2 \sin\left(\frac{2\pi n}{N}\right),$$
 (3)

the unknown phase of the wavefront $\phi(x,y)$ can be reconstructed as

$$\phi(x,y) = \arctan 2(S, C - C_0) - \mu, \tag{4}$$

where $\arctan 2(x_1, x_0)$ is defined as the angle between the 2-dimensional vector (x_0, x_1) and the x_0 axis, and $C_0 = -N |K|^2$. The value of C_0 can be readily obtained from the value of C(x, y) at the points in which the input wavefront U(x, y) is zero. Finally, the real amplitude of u(x, y) is E_0 .

III. EXPERIMENTAL SETUP

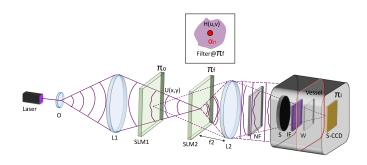


Figure 1. Experimental setup. The light source is a 405 nm cw laser diode, attenuated down to the single photon level. Lenses Ls conform a convergent optical processor. SLMs are phase-only spatial light modulators. The interferograms are detected by a Skipper CCD. The detail shows the filter placed at the Fourier Plane Πf where the central pixel of SLM2 introduces the PSI phase retardation α_n .

The experimental setup, sketched in figure 1, is basically a convergent optical processor, where two phaseonly Spatial Light Modulators (SLMs) are used: one to display the phase distribution to be measured U(x,y), and the other to dynamically introduce the phase retardation needed to implement the PSI process. The light source is a laser diode at 405 nm, that is expanded by the microscope objective O and spatially filtered by a pinhole that is imaged by lens L1 onto the Fourier plane Πf . The phase distribution U(x,y) is displayed on the phase-only SLM1, which is placed at the object plane Πo . When U(x,y) is uniform, the resulting light distribution on Πf is a bright central spot, corresponding to the Fourier transform of the entrance pupil of the system. At this position, a phase filter H(u, v), smaller than the focused spot, is displayed on SLM2. Then the phase shifts α_n needed to implement the PSI technique are introduced in the central pixel. (see inset in figure 1). This pixel is used as a perturbation to generate a spherical wave by diffraction. When the phase distribution U(x,y) is not uniform, the bright spot is deformed. Most of the light is diffracted towards higher spatial frequencies, and only the small central part of the spot goes through the phase filter. After SLM2, the lens L2 is placed at a distance equal to its focal length f2 and images the object plane onto Πi . In this way, the spherical reference wavefront, which is diffracted by the central pixel, is collimated and interferes with the tested wavefront. Finally, the interferograms are detected by the Skipper-CCD placed at the

image plane Πi . The main advantage of this convergent configuration is that it allows to change the size of the Fourier transform, to better suit the size of the PDI filter.

Both SLMs are conformed by a Sony liquid crystal television panel model LCX012BL which, in combination with polarizers and wave plates, that provide the adequate state of light polarization, allows a 2π phase modulation [16]. These liquid crystal displays have a VGA resolution of 640×480 and a pixel size of 43 μ m. Although the Skipper-CCD was hitherto only used as a particle detector [10, 17–20], in a recent paper [21] it was used for imaging purposes. This device offers ultralow readout noise and photon-number resolving capability. These features are achieved by eliminating the lowfrequency readout noise (around $2e^-$ in a conventional CCD) by multiple, nondestructive measurements (samples) of the charge in each pixel. For a readout noise of $0.2e^-$ (attained after 256 samples) the photon counting probability of misclassification is lower than 1% and can be further reduced just by increasing the number of charge samples [10]. This technology also provides the lowest dark current ($\sim 10^{-4} \text{ e}^-/\text{pixel/day}$) [20] and a full-well capacity above 33000 electrons [22] in a spatially resolved sensor with only (15x15) μm pixel size. The Skipper-CCD sensor has a total active area of 4126x886 pixels. It was designed at Lawrence Berkeley National Laboratory and manufactured by Teledyne/DALSA using high-resistivity (> $10k\Omega \cdot cm$) silicon wafers. As it operates in the temperature range of 135 to 140 K, in vacuum, the sensor is placed into a vessel that has a fused silica window (W). A dark chamber composed of a black-painted metallic holder was firmly attached to the Skipper-CCD vessel. This holder is used to place an electronic shutter (S) Melles Griot, that allows to control light exposure, and a square interferential filter (IF) centered at the laser wavelength, that avoid spurious ambient light from entering the sensor. Additionally, neutral filters (NF) are employed in order to reduce the light intensity.

After the exposition to the light for each of these phase steps, the reading process begins. This can be done in an efficient way, by selecting the amount of charge samples NSAMP desired for each region of the sensor, thus optimizating the total readout time of the measurement. The raw outcome is data in Analogical to Digital Units (ADUs) for each pixel that needs to be calibrated to number of electrons. Since the readout noise can be reduced to sub-electron values for high NSAMP, there is a closed relation between this two variables with very low probability of misclassification. The complete process for this calibration is described in [10, 21].

IV. NUMERICAL SIMULATIONS AND EXPERIMENTAL RESULTS

At very low light levels two independent problems arise. On one hand the fluctuations in number of photons

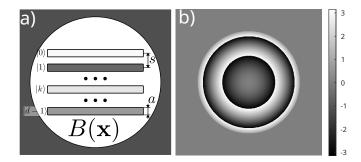


Figure 2. Programmed phases in the first SLM. a) Slit photonic qudit state case; b) Continuous lens-like phase map

becomes comparable to the average number of photons, so that, the noise coming from the light source statistics affects the accuracy of the phase estimation. On the other hand, the average number of photons is itself comparable to the readout noise of the camera used to acquire the interferograms. Thus, it is of interest to study, under these conditions, what is the average minimum number of photons per pixel that is necessary to carry out the phase reconstruction process with a certain degree of reliability. And furthermore, how this number depends on the readout noise of the camera.

In this work we explored two cases of interest: the discrete phase representing a qudit in the codification of *slit states*, and a continuous quadratic phase representing convergent lens.

A. Slits states

The first case is specially relevant for quantum information tasks. The *slits states*, whose formalism is described in detail in references [23–25], are a versatile codification that harness the spatial degrees of freedom of a single photon, to allow the creation of high dimensional quantum states. Particularly, the discretized transverse momentum of single photons defines photonic quantum states. In a previous work we showed[26] how to characterize these *slits states* with a PDI interferometric configuration.

Figure 2a shows schematically the phase distribution that represent the slits state. They consist on a phase mask with d rectangular slits of width a and length $L(\gg a,s)$, where the separation between adjacent slits is s. Thus, the resulting state is

$$|\Psi\rangle = \sum_{k=0}^{d-1} c_k |k\rangle, \tag{5}$$

where $\{|k\rangle\}_{k=0}^{d-1}$ is the logical basis, and the complex coefficients c_k represent the transmissivity and phase of each of the slits. Additionally, in order to have a light distribution similar to those usually present in an in-line holography process (small diffracting objects immersed

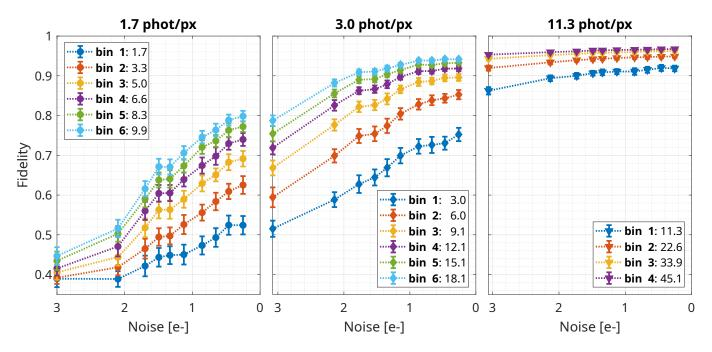


Figure 3. Reconstruction fidelity as a function of readout noise, for three different effective illuminations. a) 1.7 phot/px; b) 3.0 phot/px; c) 11 phot/px; The different curves represent effective illuminations, where the state was estimated by selecting at random n pixels for each slit.

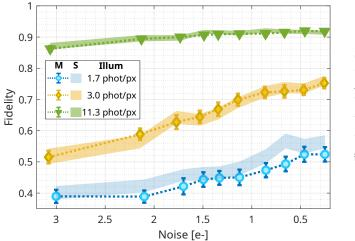
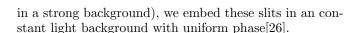


Figure 4. Measured fidelities (errorbar) and simulated (points) as a function of readout noise for three different illuminations. The errorbars represent the standard error over 100 realizations of the selection of the pixels in the region of interest of each slit.



As in this work we are focusing in phase determination, we choose a particular state with uniform intensity in each slit, of dimension d = 6, and with a phase that

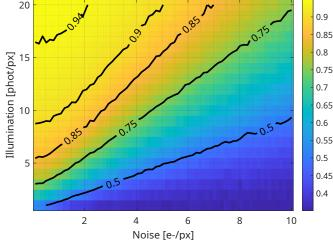


Figure 5. Simulated map of mean fidelity as a function of the total illumination and the reading noise.

increases in equal step between adjacent slits:

$$|\Psi\rangle = \frac{1}{\sqrt{6}} \sum_{k=0}^{d-1} \exp(i2\pi k/5)|k\rangle.$$
 (6)

Thus, our target state contains optical phases in all the range between 0 and 2π .

Once the phase of each pixel is estimated by Equation 4, as described in Sec. II, the state is reconstructed by at random one pixel corresponding to each of the slits, and assigning that phase value to that element of the

canonical basis. As a figure of merit we used the fidelity, that is defined, for pure states, as $F(\Phi, \Psi) = |\langle \Phi | \Psi \rangle|$, where $|\Phi\rangle$ represents the state to be prepared, and $|\Psi\rangle$ the state that is reconstructed [27].

We reconstructed this state for three levels of illumination: 1.7 phot/px, 3.0 phot/px, and 11.3 phot/px. Where the illumination was estimated as the intensity averaged over all the pixels in the region defined by the slits (~ 600). However, in order to study other values of illumination, we considered the n-pixel (binning of n pixels) averaged state, where the state determination was made by averaging the phase for n randomly chosen pixels in the region of each of the slits. In this case we defined the effective illumination as being n times the real illumination per pixel. To estimate the mean value of the fidelity, and its dispersion in each case, we perform a boostrap method: for each level of noise and binning n, we sampled without repetition 81 states, to get an average fidelity. This process was repeated 64 times to obtain the mean value of these averaged fidelities, and its standard deviation.

Figure 3 shows how the reconstruction fidelity changes with the readout noise, for the three cases of real illumination. Each of the curves in a single plot, represent the effective illumination, that was obtained by binning n pixel for each of the slit regions, to determine the phase of said slit. It is clear from these plots the improvement in the fidelity attained by increasing the number of samples in the Skipper CCD mode. The highest readout noise corresponds to NSAMP = 1 samples in the Skipper CCD ($\sim 3e^-$), while the smallest readout noise corresponds to NSAMP = 144 samples ($\sim 0.2e^-$).

In all cases the reduction in the readout noise leads to an increase on the fidelity reconstruction. However, for the lowest level of illumination, 1.7 phot/px, maximum achieved fidelity for 1 bin is about .5, pointing that this number of photons is not sufficient to determine the phase. The fidelity in this case can be improved by averaging the phase over more pixels, and thus incrementing the effective illumination. However, there is a striking difference with the other two levels of illumination. For the 3.0 phot/px, the 1 bin case can achieve more than .75 of fidelity when readout noise is decreased well below one e^- . And a binning greater or equal to 2 is enough to get mean reconstruction fidelities over .8, for the same readout noise condition. In the last case, with over 11 phot/px,, the worst scenario corresponds to a fidelity that is already over .85, and the improvements are smaller both with the increased binning and the decrease in the readout noise. This is expected, both the relative effect of Poissonian fluctuations and that of the readout noise are much smaller.

1. Simulation

To perform the simulation, for each configuration of light level, synthetic interferograms were generated according to the equation 1. To account for the Poissonian noise characteristic of the photon statistic of a highly attenuated coherent state, we sampled, for each of the pixels of each of the interferograms, a Poissonian distribution with the mean value corresponding to the intensity value of said pixel. And additional Gaussian noise is added to each pixel, with zero mean and standard deviation equal to the electronic noise, to represent the readout noise of the camera.

Figure 4 compares the measured and the simulated fidelity reconstruction as a function of the readout noise of the camera, for three different examples of illumination: 1.7 phot/px, 3.0 phot/px, and 11.3 phot/px. In this case, the binning was n=1, and the random sampled was repeated 100 times. The continuous line represents he average fidelity over the repetitions, while the error bars represent the standard error. On the other hand, the point represents the simulated reconstruction fidelity, averaged over 2000 repetitions. For the two highest illuminations, the noise model is in excellent agreement with the measurements. In the case of the lowest illumination level, the simulated mean fidelity it is consistently above the value estimated experimentally, but the confidence band overlap for most of the points.

Thus, this noise model is a useful tool to estimate what is the expected reconstruction fidelity, given the level of illumination and the readout noise of the detector used. In that regard, Figure 5 shows the mean fidelity map as a function of the electronic noise and the mean illumination, where in each point is an average over 2000 repetitions. To asses this fidelity for another dimension, the similar map can be generated using the same statistical model.

It should be noted that our analysis is based on raw images, that is, we do not use maximum likelihood algorithms [28] to improve them, nor do we apply principles of image compression and associated image reconstruction [29]. We also do not improve the sensitivity of the measurement by using photon-subtracted thermal states [30].

B. Measurement of an arbitrary phase distribution

Another case of interest is that of the determination of an arbitrary phase distribution. In order to study this case, we programmed in the SLM1 a lens-like phase, i.e., a quadratic phase, as represented schematically in Figure 2b.

As in this case we can not define regions of constant phase, to asses the quality of the phase reconstruction, we compare the obtained phase map with a reference one, that was obtained with high light intensity ($\sim 500~{\rm phot/px}$, where both the Poissoinan and the readout noise are negligible).

The upper row of Figure 6 shows the histogram of the phase differences for three different illuminations: 1.9 phot/px, 4.5 phot/px, and 12.7 phot/px, and the two

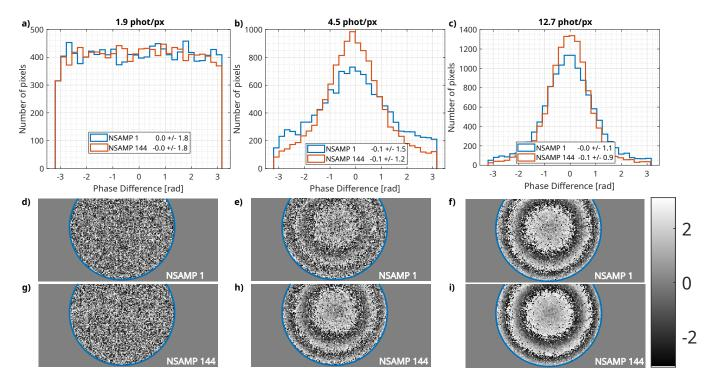


Figure 6. Each column shows, for a fixed illumtion intensity, the histogram of phase difference in each pixel for a lens-like phase wavefront (top row), the corresponding phase map for NSAMP=1 (middle row), and for NSAMP=144 (bottom row). Panels a,d,g) 1.9 phot/px; b,e,h) 4.0 phot/px; c,f,i) 12.7 phot/px;

lines in each histogram corresponds to the measurement without Skipper CCD mode (NSAMP = 1) and with (NSAMP = 144). The lower rows show a comparison between the reconstructed phase maps for the minimum (NSAMP = 1, medium row) and the maximum number (NSAMP = 144, bottom row) of Skipper CCD samples that we used. It is worth noting that the quality of the reconstruction for 1.9 phot/px, (Figure 6a) does not improve even when reducing the readout noise well below the one e^- level. This is consistent with the results that we got in the discrete case (Figure 3a - bin 1), where with approximately the same level of illumination, the reconstruction fidelity could not be increased more than \sim .5.

Instead, for the cases of Figures 6b and 6c, there is a improvement in the phase estimation with the number of Skipper CCD samples, reflected in a decrease of ~ 20 % in the standard deviation of the phase difference. In these two cases, a clear improvement in the phase map can be seen as the readout noise is reduced. However, for the 12.7 phot/px case, the improvement is smaller, as both the readout noise and the Poissonian noise start to be significantly lower than the mean intensity.

Thus, the phase determination can be significantly improved by reducing the readout noise, by taking advantage of the Skipper mode, for medium illumination levels, between 4 and 15 photons per pixel approximately. Interestingly, even when the readout noise is negligible, as is the case with the Skipper CCD camera, still a light level slightly higher than 4 photons per pixels is needed

to reconstruct phases.

V. CONCLUSIONS

In this work we studied how interferometric phase reconstruction is affected by the two main sources of noise for highly attenuated coherent illumination: the readout noise of the detector used to record the interferograms, and the shot noise of the illumination.

We reconstructed the phase of several wavefronts with a combination of a point diffraction interferometer and phase shifting interferometry, where the detection was done by Skipper-CCD camera. Allowing us to select, and even eliminate the readout noise.

On one hand we performed the reconstruction of a spatial distribution with d=6 uniform phase regions that encode a d-dimensional qudit. In this case, we showed an improvement in the reconstruction fidelity with the reduction of the readout noise for all the illumination levels. However, even with in the absence of readout noise, with under 3 phot/px it was not possible to reconstruct states with a fidelity over .8. In this particular case, we propose a noise model to predict the expected fidelity reconstruction as a function of both the readout noise level, and the mean number of photons, that is consistent with the experimental results.

On the other hand, we reconstructed a continuous phase, showcasing phase reconstruction under low illumination for arbitrary phases. In a similar manner to the discrete case, the quality of the reconstruction was improved by the reduction of the readout noise for illuminations greater than 4 phot/px. And likewise, even in the absence of readout noise, non meaningful phase could be estimated with less than 3 phot/px.

ACKNOWLEDGMENTS

This work was supported by Fermilab under DOE Contract No. DE-AC02-07CH11359. The CCD devel-

opment work was supported in part by the Director, Office of Science, of the DOE under No. DE-AC02-05CH11231. CI and QPS acknowledges the support of the Secretaría de Ciencia y Técnica, Universidad de Buenos Aires (20020170100564BA), of the Consejo Nacional de Investigaciones Científicas y Técnicas (PIP 2330), and of the Ministerio de Ciencia Tecnologia e Innovacion/Agencia Nacional de Promocion Científica y Tecnologica (PICT-2020-SERIEA-02031). QPS was supported by a CONICET Fellowship.

- [1] D. Malacara, Optical Shop Testing (Wiley, 2007).
- [2] U. Schnars and W. Jüptner, Appl. Opt. 33, 179 (1994).
- [3] M. K. Kim, J. Photon. Energy, 018005 (2010).
- [4] J. Kacperski and M. Kujawinska, Opt. Express 14, 9664 (2006).
- [5] H. Zhang, F. A. Monroy-Ramírez, A. Lizana, C. Iemmi, N. Bennis, P. Morawiak, W. Piecek, and J. Campos, Optics and Lasers in Engineering 113, 71 (2019).
- [6] Q. Pears Stefano, L. Rebón, S. Ledesma, and C. Iemmi, Phys. Rev. A 96, 1 (2017), 1707.03306.
- [7] V. Giovannetti, S. Lloyd, and L. Maccone, Science 306, 1330 (2004).
- [8] M. W. Mitchell, J. S. Lundeen, and A. M. Steinberg, Nature 429, 161 (2004).
- [9] J. Tiffenberg, M. Sofo-Haro, A. Drlica-Wagner, R. Essig, Y. Guardincerri, S. Holland, T. Volansky, and T.-T. Yu, Phys. Rev. Lett. 119, 131802 (2017).
- [10] D. Rodrigues, K. Andersson, M. Cababie, A. Donadon, A. Botti, G. Cancelo, J. Estrada, G. Fernandez-Moroni, R. Piegaia, M. Senger, M. S. Haro, L. Stefanazzi, J. Tiffenberg, and S. Uemura, Nuclear Instruments and Methods in Physics Research, Section A: Accelerators, Spectrometers, Detectors and Associated Equipment 1010, 10.1016/j.nima.2021.165511 (2021), 2004.11499.
- [11] K. Creath, Progress in Optics 26, 349 (1988).
- [12] W. Linnik, in *Dokl. Akad. Nauk*, SSSR, Vol. 1 (1933) pp. 21–33.
- [13] C. R. Mercer and K. Creath, Appl. Opt. 35, 1633 (1996).
- [14] C. Iemmi, A. Moreno, J. Nicolás, and J. Campos, Opt. Lett. 28, 1117 (2003).
- [15] C. Ramírez, E. Otón, C. Iemmi, I. Moreno, N. Bennis, J. M. Otón, and J. Campos, Opt. Express 21, 8116 (2013).
- [16] A. Márquez, C. Iemmi, I. Moreno, J. A. Davis, J. Campos, and M. J. Yzuel, Opt. Eng 40, 2558 (2001).
- [17] L. Barak, I. M. Bloch, M. Cababie, G. Cancelo, L. Chaplinsky, F. Chierchie, M. Crisler, A. Drlica-Wagner, R. Essig, J. Estrada, E. Etzion, G. F. Moroni, D. Gift, S. Munagavalasa, A. Orly, D. Rodrigues, A. Singal, M. S. Haro, L. Stefanazzi, J. Tiffenberg, S. Uemura, T. Volansky, and T.-T. Y. and, Phys. Rev. Lett. 125, 10.1103/phys-

- revlett.125.171802 (2020).
- [18] N. Castelló-Mor (DAMIC-M), Nucl. Instrum. Meth. A 958, 162933 (2020), 2001.01476.
- [19] A. Aguilar-Arevalo et al. (CONNIE), JHEP 2022 (17), 017, 2110.13033.
- [20] L. Barak, I. M. Bloch, A. Botti, M. Cababie, G. Cancelo, L. Chaplinsky, F. Chierchie, M. Crisler, A. Drlica-Wagner, R. Essig, J. Estrada, E. Etzion, G. Fernandez Moroni, D. Gift, S. E. Holland, S. Munagavalasa, A. Orly, D. Rodrigues, A. Singal, M. S. Haro, L. Stefanazzi, J. Tiffenberg, S. Uemura, T. Volansky, and T.-T. Yu (SENSEI Collaboration), Phys. Rev. Applied 17, 014022 (2022).
- [21] Q. Pears Stefano, A. Magnoni, J. Estrada, C. Iemmi, D. Rodrigues, and J. Tiffenberg, Phys. Rev. Applied 19, 064044 (2023).
- [22] A. Drlica-Wagner, E. M. Villalpando, J. O'Neil, J. Estrada, S. Holland, N. Kurinsky, T. Li, G. F. Moroni, J. Tiffenberg, and S. Uemura, Proc. SPIE Int. Soc. Opt. Eng. 11454, 114541A (2020).
- [23] L. Neves, S. Pádua, and C. Saavedra, Phys. Rev. A 69, 10.1103/PhysRevA.69.042305 (2004).
- [24] M. A. Solís-Prosser, A. Arias, J. J. M. Varga, L. Rebón, S. Ledesma, C. Iemmi, and L. Neves, Opt. Lett. 38, 4762 (2013).
- [25] J. J. Varga, S. Ledesma, C. Iemmi, and L. Rebón, Phys. Rev. A 96, 34 (2017), 1706.00920v1.
- [26] Q. Pears Stefano, L. Rebón, and C. Iemmi, J. Opt. 22, 10.1088/2040-8986/abbb5c (2020), 2005.09963.
- [27] M. A. Nielsen and I. L. Chuang, Quantum Computing and Quantum Information (Cambridge University Press, 2000).
- [28] D. A. Barmherzig and J. Sun, Opt. Express 30, 6886 (2022).
- [29] P. A. Morris, R. S. Aspden, J. E. C. Bell, R. W. Boyd, and M. J. Padgett, Nat. Commun. 6, 5913 (2015).
- [30] S. M. Hashemi Rafsanjani, M. Mirhosseini, O. S. Magaña-Loaiza, B. T. Gard, R. Birrittella, B. E. Koltenbah, C. G. Parazzoli, B. A. Capron, C. C. Gerry, J. P. Dowling, and R. W. Boyd, Optica 4, 487 (2017).